

On Detection of a Wave Age Dependency for the Sea Surface Roughness

B. LANGE*

Risø National Laboratory, Roskilde, Denmark

H. K. JOHNSON

DHI Water & Environment, Hørsholm, Denmark

S. LARSEN AND J. HØJSTRUP

Risø National Laboratory, Roskilde, Denmark

H. KOFOED-HANSEN

DHI Water & Environment, Hørsholm, Denmark

M. J. YELLAND

Southampton Oceanography Centre, Southampton, United Kingdom

(Manuscript received 5 February 2003, in final form 1 December 2003)

ABSTRACT

The wave age dependency of the nondimensional sea surface roughness (also called the Charnock parameter) is investigated with data from the new field measurement program at Rødsand in the Danish Baltic Sea. An increasing Charnock parameter with inverse wave age is found, which can be described by a power-law relation. Friction velocity is a common quantity in both the Charnock parameter and wave age. Thus self-correlation effects are unavoidable in the relation between them. The significance of self-correlation is investigated by employing an artificial “dataset” with randomized wave parameters. It is found that self-correlation severely influences the relation. For the Rødsand dataset the difference between real and randomized “data” was found to be within the measurement uncertainty. By using a small subset of the data it was found that the importance of self-correlation increases for a narrower range of wave age values. This supports the conclusion of Johnson et al. that because of the scatter and self-correlation problems the coefficients of the power-law relation can only be obtained from the analysis of an aggregated dataset with a wide wave age range combining measurements from several sites. The dependency between wave age and sea roughness has been discussed extensively in the literature with different and sometimes conflicting results. A wide range of coefficients has been found for the power-law relation between the Charnock parameter and wave age for different datasets. It is shown that self-correlation contributes to such differences, since it depends on the range of wave age values present in the datasets. Also, data are often selected for rough flow conditions with the Reynolds roughness number. It is shown that for datasets with large scatter this can lead to misleading results with regard to the relationship between wave age and Charnock parameter. Two different methods to overcome this problem are presented.

1. Introduction

The momentum transfer from the marine atmospheric boundary layer to the wind-driven water waves is important for all processes of air–sea interaction, such as

wind wave growth, storm surges, and atmospheric circulation. It depends on the aerodynamic sea surface roughness, which is therefore one of the most important quantities for the description of the physical processes on both sides of the air–sea interface.

Using dimensional arguments, Charnock (1955) suggested that the dimensionless sea roughness gz_0/u_*^2 (also called the Charnock parameter z_{ch}) is constant, where g is the gravitational acceleration, z_0 is the sea surface roughness, and u_* is the friction velocity. Various field measurements showed that this is a reasonable concept for open-ocean sites, except for very low wind speeds

* Current affiliation: University of Oldenburg, Oldenburg, Germany.

Corresponding author address: Bernhard Lange, Energy and Semiconductor Research Laboratory, Dept. of Physics, University of Oldenburg, D-26111 Oldenburg, Germany.
E-mail: Bernhard.Lange@uni-oldenburg.de

($<3\text{--}4\text{ m s}^{-1}$), although some increase of the Charnock parameter with wind speed has been found (see, e.g., Yelland and Taylor 1996). For sites near the coast, the Charnock parameter has been found to vary from site to site. Thus, z_{ch} is not a constant but depends on other geophysical parameters. It has been argued that these other parameters are properties of the wave field, that is, that the sea surface roughness is not only dependent on wind speed, but also on the wave field present, which in turn is governed by wind, fetch, and water depth. Different attempts have been made to establish a relationship between the sea surface roughness and different properties of the wave field like wave height, wave steepness, or wave age (e.g., Hsu 1974; Donelan 1990; Smith et al. 1992; Taylor and Yelland 2001). However, though there is general consensus that the sea surface roughness depends on the wave field, the quantities suitable for description of this dependence are still a subject of controversy.

Most authors have tried to improve the description of the sea surface roughness by a parameterization of the Charnock parameter with wave age (e.g., Smith et al. 1992; Donelan et al. 1993; Johnson et al. 1998, hereinafter JHVL). JHVL showed that under specific conditions (discussed in section 2e) the Charnock parameter depends only on wave age. They describe this dependence with a power law between the Charnock parameter (or normalized sea surface roughness), z_{ch} , and the inverse wave age, u_*/c_p , in the form

$$z_{\text{ch}} = A \left(\frac{u_*}{c_p} \right)^B. \quad (1)$$

From an empirical fit to measurements from the Risø Air Sea Experiment (RASEX) together with other previously measured datasets they find the coefficients $A = 1.89$ and $B = 1.59$. One of the main problems in these results was the conflicting, apparent trend of decreasing Charnock parameter with inverse wave age in the RASEX dataset taken alone (see also Taylor and Yelland 2001).

The problem with this kind of scaling is that the two quantities, Charnock parameter and wave age, between which a functional relationship is proposed are not independent of each other. This can lead to self-correlation problems; that is, the functional relationship might be distorted or even determined by the common scaling variable. A theoretical analysis of the self-correlation problem has been presented by Hicks (1978) and specifically for the question of the wave-age-dependent Charnock parameter by Smith et al. (1992). The latter group concluded that self-correlation had an influence on the results of the Humidity Exchange over the Sea (HEXOS) experiment data. JHVL generalized that this will always be the case for a given site where the fetch range is limited. They concluded that the combination of data from several sites is necessary to minimize self-

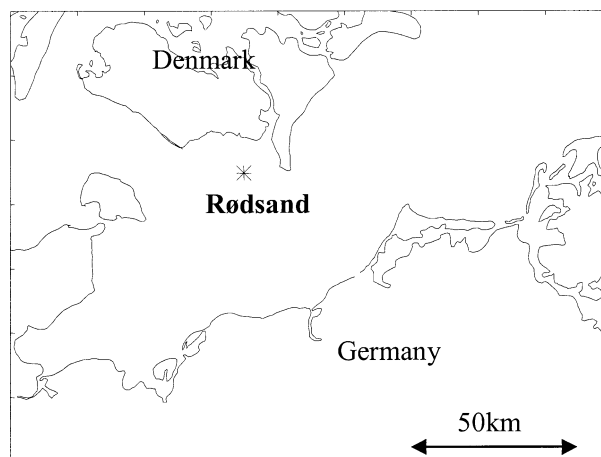


FIG. 1. Rødsand measurement site.

correlation. This conclusion is also supported by a recent study by Drennan et al. (2003).

In the present paper we follow the JHVL approach with three principal aims:

- 1) to test the relation proposed by JHVL with a new, independent dataset,
- 2) to investigate the influence of self-correlation on the relation, and
- 3) to contribute to an understanding of the reasons for the conflicting results found by JHVL and in the literature (see, e.g., Toba et al. 1990; Drennan et al. 2003; Maat et al. 1991) by investigating how self-correlation and the data analysis method could influence the resulting trend.

The plan of the paper is as follows. In section 2 the Rødsand field measurement program is presented and the preparation of the measured data is described. In section 3 these data are analyzed in different ways. The results are compared with each other and with published results. The influence of self-correlation on the relation is investigated in section 4. The data analysis method is discussed in section 5 to gain a better understanding of the relationship between the Charnock parameter and wave age. In the final section 6 the conclusions of the paper are summarized.

2. The Rødsand field measurement program

a. Site

A 50-m-high meteorological measurement mast was established at Rødsand in October 1996 as part of a Danish study of wind conditions for proposed offshore wind farms. Simultaneous wind and wave measurements were performed starting in April 1998. The mast is situated about 11 km south of the island Lolland in Denmark (54.540°N , 11.745°E). The location of the mast is shown in Fig. 1. The mast is located in 7.7-m mean water depth with an upstream fetch from 30 to

TABLE 1. Instrumentation for the Rødsand measurements.

Parameter	Height (m MSL)	Instrument	Sampling rate
Wind speed	50.3	Cup anemometer	5 Hz
	29.8	Cup anemometer	5 Hz
	10.2	Cup anemometer	5 Hz
Wind direction	29.7	Wind vane	5 Hz
Three-axis wind speed and temperature	46.6 (42.3 m after 12 May 1999)	Ultrasonic anemometer	20 Hz
Air temperature	10.0	Pt 100	30-min mean
Temperature difference	49.8–10.0	Pt 500	30-min mean
Sea temperature		Pt 100	30-min mean
Sea level		DHI AWR201 acoustic wave recorder	8 Hz
Sea current		GMI current meter	8 Hz

100 km (and above) from the SE to WNW sector (120° – 290°). The water depth slowly increases to an average upstream depth of about 20–25 m in this sector. In the NW to N sector (300° – 350°), the water depth is relatively shallower (from 1 to 7 m) and the fetch is shorter (about 10–20 km).

b. Instrumentation and measurements

The instrumentation of the measurement mast is listed in Table 1. Wave and current data are collected simultaneously with several atmospheric parameters. About 5900 half-hourly records with simultaneous wind and wave measurements have been recorded. A more detailed description of the instrumentation and data can be found in Lange et al. (2001).

1) CUP ANEMOMETERS

Mean wind speeds and variances are derived from cup anemometers located at three heights (see Table 1). Calibrated instruments of the type Risø P2546a are used. The calibration accuracy is estimated to be $\pm 1\%$. Data are corrected for flow distortion errors due to the structure on which the anemometer is mounted, that is, the mast and the booms [see section 2d(2)]. However, a correction uncertainty remains, and the overall uncertainty of the wind speed measurement with cup anemometers is estimated to be $\pm 3\%$.

2) WIND VANE

A wind vane of the type Risø Aa 3590 is used. The uncertainty of the instrument itself is negligible. However, the adjustment of the orientation of the instrument is difficult in the field and the absolute accuracy is estimated to be about $\pm 5^{\circ}$.

3) SONIC ANEMOMETER

The sonic anemometer is of the type Gill F2360a and is mounted at 46.6-m height (42.3 m from 12 May 1999) above mean sea level (MSL). It measures wind speed

in three components (x , y , z) and air temperature with a resolution of 20 Hz. Fluxes are calculated after turning the coordinate system such that the mean bias in the vertical and crosswind components are zero. Remaining biases were found to be very small (below 1 cm s^{-1}) and were neglected.

Errors due to flow distortion of the measuring mast have been corrected [see section 2d(2)], although remaining errors have to be expected, especially for friction velocity measurements. Additionally, sonic anemometers experience an array flow distortion since transducers and struts of the instrument distort the wind flow in the measurement volume. For the horizontal wind speed component flow distortions are corrected with an individual calibration curve supplied by the manufacturer. This is not the case for the vertical wind component. Mortensen and Højstrup (1995) report systematic differences in a field experiment of typically 5% in mean wind speed and 10%–15% in friction velocity between different sonic anemometer types. From wind tunnel measurements they find that the errors are dependent on temperature and mean wind direction. However, they state that further investigations are necessary before a correction method can be established. Therefore no attempt has been made to correct the measurements of the sonic anemometer for array flow distortion. The estimated accuracy for the horizontal wind speed component is about $\pm 5\%$. For the friction velocity derived by eddy correlation it is $\pm 10\%$. Both errors are expected to contain a wind-direction-dependent bias.

Additionally statistical errors due to sampling variability have to be considered, which are responsible for the scatter in the data. Using the approximation of Wyngaard (1973) derived from the Kansas data, the expected accuracy for the u_* measurements is about 10% for an eddy-correlation measurement at 45-m height with an averaging time of 30 min and a mean wind speed of 10 m s^{-1} . It is mainly this sampling variability that is responsible for the unavoidable scatter in the u_* data.

4) ACOUSTIC WAVE RECORDER

Waves are measured by an acoustic wave recorder (AWR), which is a sonar-type instrument positioned un-

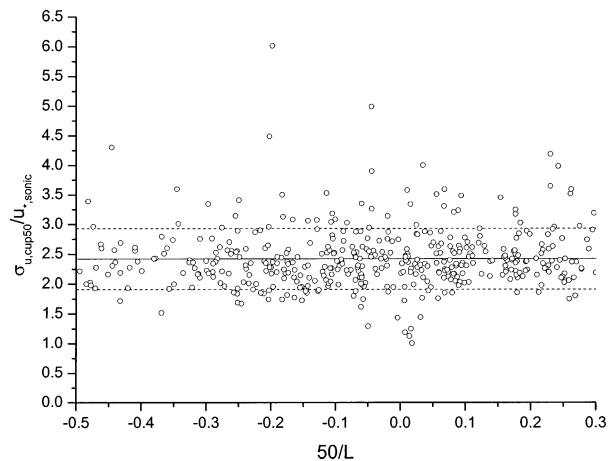


FIG. 2. Ratio of standard deviation measured with the cup anemometer at 50-m height and friction velocity derived from the sonic anemometer at 46.6-m (42.3 m) height vs stability parameter $50/L$; horizontal lines show the mean ratio (2.42) and its standard deviation (0.51).

der water on a support structure. The type is the HD-AWR201 from DHI Water & Environment.

The instrument has been located about 100 m southwest of the offshore meteorological mast at Rødsand since March 1998. The instrument was placed 3.74 m above the sea bottom; the average water level during the measurement was 7.7 m. The instrument measures the distance from the acoustic transducer to the water surface with a sampling rate of 8 Hz.

The cutoff frequency of the instrument is determined by its spatial resolution (area sampled by the acoustic transducer at the surface) rather than its sampling rate. It is estimated to be about 0.8 Hz. The measured time series of water-level fluctuations was passed through a simple filter in order to remove local spikes in the data. A fixed speed of sound (1475 m s^{-1}) is used, independent of actual water temperature and salinity. Water temperature and salinity ranges have been estimated for the site. They lead to a maximum measurement error of -4% to $+1\%$ in the water-level value and wave height.

5) WATER CURRENT MEASUREMENT

The water current sensor is a two-dimensional electromagnetic sensor measuring the water velocity in the x and y directions, manufactured by Geological and Marine Instrumentation (GMI, Kvistgaard, Denmark, now EIVA a/s). It is located 5.3 m above the sea bottom. The measurement accuracy of the sensor is estimated to be $\pm 2\%$.

c. Derived measured quantities

1) FRICTION VELOCITY

Covariances are calculated from the sonic anemometer measurements. Linear trends remaining in the time

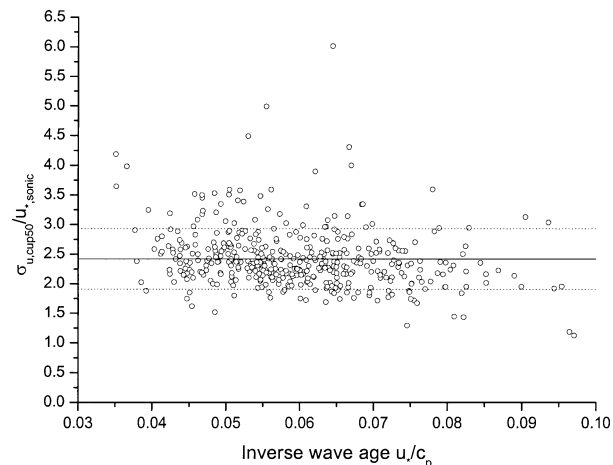


FIG. 3. As in Fig. 2 but vs inverse wave age u_*/c_p .

series after selection for stationary conditions (see section 2e) are removed before calculation of the covariances. Friction velocity is calculated with the eddy-correlation method as

$$u_* = (\overline{u'w'^2} + \overline{v'w'^2})^{0.25}. \quad (2)$$

The uncertainty in the friction velocity measurement is estimated to be about $\pm 10\%$ as a combination of the general measurement uncertainty of the instrument and a direction-dependent error due to flow distortion.

If the direction-dependent error coincides with a wind-direction-dependent distribution of wave ages in the data, this error can distort the trend of sea surface roughness with wave age. This is investigated by comparing the observed trend with the one found in an analysis without using the sonic anemometer, where the friction velocity is derived from the wind speed variance measurement of a cup anemometer.

For near-neutral atmospheric stability, friction velocity u_* and standard deviation of the wind speed σ_u are proportional:

$$u_* = \frac{\sigma_u}{C}. \quad (3)$$

The constant C is estimated for the Rødsand dataset by comparing the standard deviation measured with the cup anemometer at 50-m height and the friction velocity derived from the sonic anemometer at 46.6-m (42.3 m) height. The ratio of both is plotted versus the stability parameter $50/L$ in Fig. 2. No dependence on atmospheric stability can be found for the near-neutral stability range used. A possible dependence of C on wave age, which could distort the trend of the Charnock parameter versus wave age, is investigated in Fig. 3. A weak dependence of decreasing C with increasing inverse wave age is found. It has no significant effect on the trend of the Charnock parameter versus wave age and can be neglected. The mean value for C is 2.42 with a standard deviation of 0.51, which is about 20%. This is in the

range of commonly used values: Garratt (1992) quotes 2.4 for flat terrain, and Stull (1988) lists values from 2.47 to 2.57.

The measured value for C is used to derive friction velocities from the three cup anemometer measurements. They provide complementary indirect measurements of the friction velocity, which are expected to have no wind-direction-dependent error.

2) NEUTRAL WIND SPEED AT 10-M HEIGHT

The measured mean wind speed has been corrected for influences of the atmospheric stability, described by the Monin–Obukov length L . This L has been determined from the measurements of the friction velocity u_* , the heat flux $w'\Theta'$, and the potential temperature Θ at 10 m:

$$L = -u_*^3 / \left(\kappa \frac{g}{\Theta} \overline{w'\Theta'} \right). \quad (4)$$

The von Kármán constant κ is taken as 0.4 and the gravitational constant g as 9.81 m s^{-2} . The error in L due to humidity can be neglected since the humidity influence is to a large degree included in the heat flux measurement of the sonic anemometer, which measures the sound virtual temperature (see, e.g., Schotanus et al. 1983). The stability function Ψ is calculated following the standard approach (see, e.g., Geernaert et al. 1986; JHVL), and the neutral wind speed u_{10n} is derived from the measured wind speed u_{10} by

$$u_{10n} = u_{10} + \frac{u_*}{\kappa} \Psi \left(\frac{10}{L} \right). \quad (5)$$

Deviations of the measurement height from 10 m due to water-level variations have been accounted for by a log–linear wind profile with Charnock sea surface roughness (with $z_{\text{ch}} = 0.018$) and the measured stability parameter.

3) SEA SURFACE ROUGHNESS

For the calculation of sea surface roughness the measurements of friction velocity u_* , either from sonic or cup anemometer measurements [see section 2c(1)], and of the neutral wind speed at 10-m height, u_{10n} , have been used. The friction velocity has been corrected to its surface value [see section 2d(1)]. The roughness length is calculated from the logarithmic wind profile:

$$z_0 = z / \exp \left[\frac{u_n(z)\kappa}{u_*} \right]. \quad (6)$$

The dimensionless sea surface roughness or Charnock parameter is defined as

$$z_{\text{ch}} = \frac{z_0 g}{u_*^2} = g z / \left\{ u_*^2 \exp \left[\frac{u_n(z)\kappa}{u_*} \right] \right\}. \quad (7)$$

4) WAVE HEIGHT, WAVE PERIODS, AND WAVE SPECTRUM BANDWIDTH

All wave parameters have been derived from the time series of water elevation measured by the AWR. The significant wave height H_s is derived from the standard deviation of the water level σ by

$$H_s = 4\sigma. \quad (8)$$

Three different wave periods and the bandwidth of the spectrum are derived from the wave spectrum calculated for each 30-min wave record measured at Rødsand. The wave period at the 50% accumulated variance T_{50} has been calculated as

$$T_{50} = 1/f_{50}, \quad (9)$$

the mean period T_m as

$$T_m = m_0/m_1, \quad (10)$$

and the mean period based on zero-crossing frequency T_z as

$$T_z = \sqrt{m_0/m_2}. \quad (11)$$

The bandwidth of the wave spectrum has been found from

$$\text{bw} = \log_{10}(f_{75}/f_{25}). \quad (12)$$

In the equations, m_n denotes the n th moment of the spectrum and f_n is the frequency at $n\%$ variance.

5) WAVE PHASE SPEED AT PEAK FREQUENCY

The spectral peak frequency f_p is determined from the measured wave spectra. The direct way of finding f_p would be to search for the frequency corresponding to the maximum spectral density. However, this method is very sensitive to noise. Therefore, following JHVL, the statistically more stable frequency at 50% accumulated variance f_{50} is determined first and the measured f_{50} is then converted to f_p by using a mean wave spectrum shape.

The Joint North Sea Wave Project (JONSWAP) spectral model (Hasselmann et al. 1973) is used as a shape function to find the average ratio f_{50}/f_p that best fits the measured spectra. The average values of the parameters for the fitted spectrum are $\gamma = 1.58$ (the peakedness parameter), $f_{50}/f_p = 1.11$, $\text{bw} = 0.153$, and $T_m/T_z = 1.081$. These values compare well to the measured bandwidth and time-scale ratio as shown in Figs. 4 and 5, respectively. The phase speed at peak frequency c_p is calculated using the measured water depth and spectral peak frequency f_p in the linear dispersion relation.

d. Data corrections

1) CORRECTION OF THE WIND STRESS MEASUREMENT FOR ELEVATION

To a first approximation it is usually assumed that the flux in the surface layer is independent of height, im-

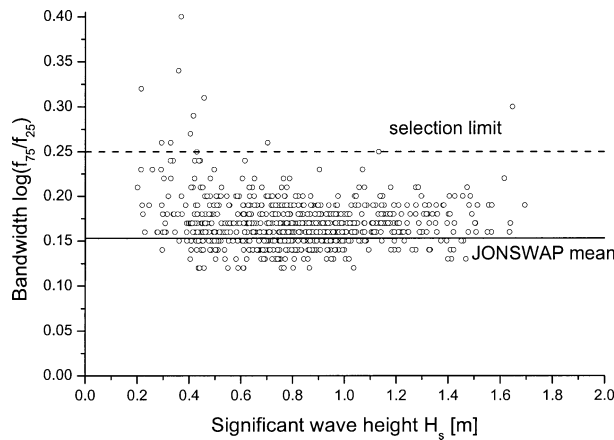


FIG. 4. Bandwidth of the measured data at Rødsand vs significant wave height; also shown is the bandwidth of the fitted JONSWAP spectrum (0.15) and the bandwidth limit used to select single-peaked spectra (0.25).

plying that the friction velocity is constant. However, this assumption is not entirely correct and for near-neutral and stable conditions the friction velocity decreases slightly with height. Since the determination of the sea surface roughness is very sensitive to the value of the friction velocity, this deviation is accounted for in the determination of the surface friction velocity.

Donelan (1990) derives the following expression from an analysis of the horizontal momentum equation at the surface and the top of the boundary layer, when no observed boundary layer height is available:

$$u_*(z) = \sqrt{u_{*,s}^2 \left(1 - \frac{\alpha_0 f_c z}{u_{*,s}} \right)}, \quad (13)$$

where $u_*(z)$ is the friction velocity measured at height z , $u_{*,s}$ is the friction velocity at the surface, $\alpha_0 = v_g/u_{*,s}$ is the ratio of geostrophic wind v_g and $u_{*,s}$ (taken

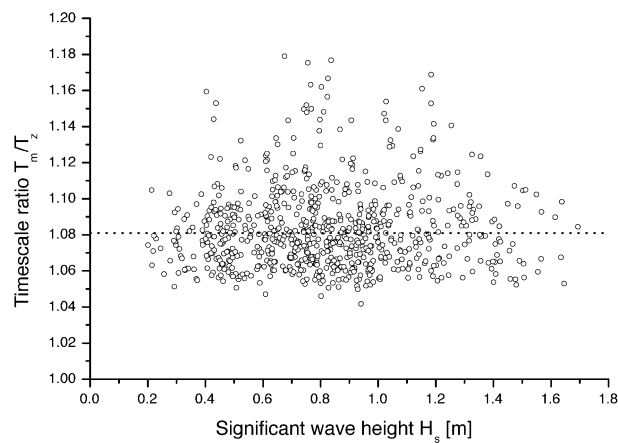


FIG. 5. Ratio of mean period and wave period based on zero-crossing frequency of the measured data at Rødsand vs significant wave height; also shown is the time-scale ratio of the fitted JONSWAP spectrum.

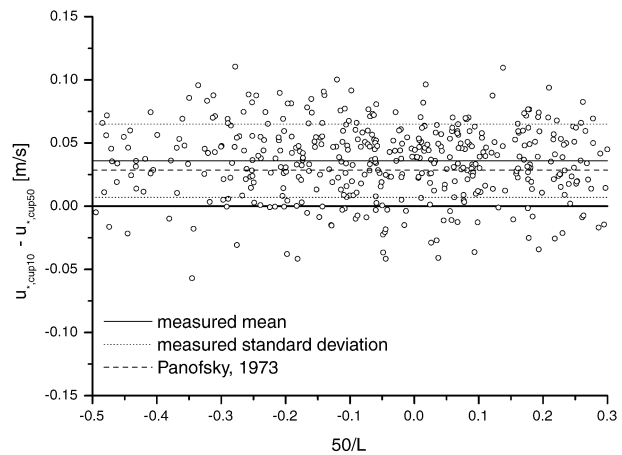


FIG. 6. Difference between friction velocities derived from cup anemometer standard deviations at 10- and 50-m height vs stability parameter; horizontal lines show the mean difference (0.036 m s^{-1}), its standard deviation (0.029 m s^{-1}), and the mean result of Eq. (13).

as $\alpha_0 = 12$), and f_c is the Coriolis parameter ($1.46 \times 10^{-4} \sin \phi$, with ϕ being latitude).

A direct comparison of this equation with measured friction velocities cannot be made with the Rødsand dataset since a sonic anemometer is only available at one height. However, friction velocities derived from cup anemometer measurements of wind speed variances at the three heights 10, 30, and 50 m can be compared. The difference between friction velocities derived from cup anemometer variances at 10- and 50-m height versus the stability parameter is shown in Fig. 6; the difference between 10 and 30 m is shown in Fig. 7. A height dependence of the friction velocity is observed that is independent of stability for the near-neutral stability range used. The mean difference over the height difference of 40.1 m is 0.036 m s^{-1} (i.e., $0.0009 \text{ m s}^{-1} \text{ m}^{-1}$); over the height difference of 19.6 m it is 0.021

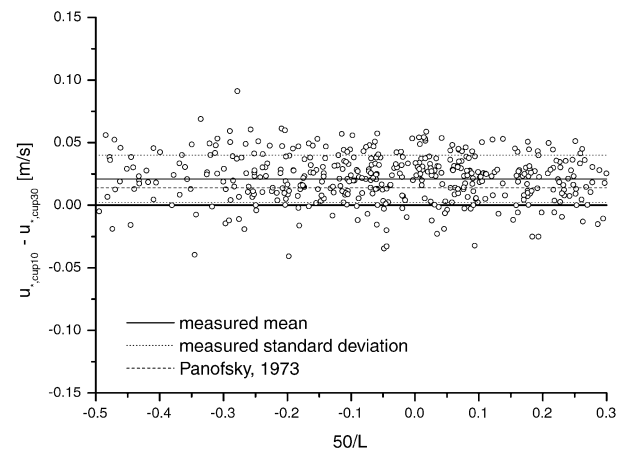


FIG. 7. Difference between friction velocities derived from cup anemometer variances at 10- and 30-m height vs stability parameter; horizontal lines show the mean difference (0.021 m s^{-1}), its standard deviation (0.019 m s^{-1}), and the mean result of Eq. (13).

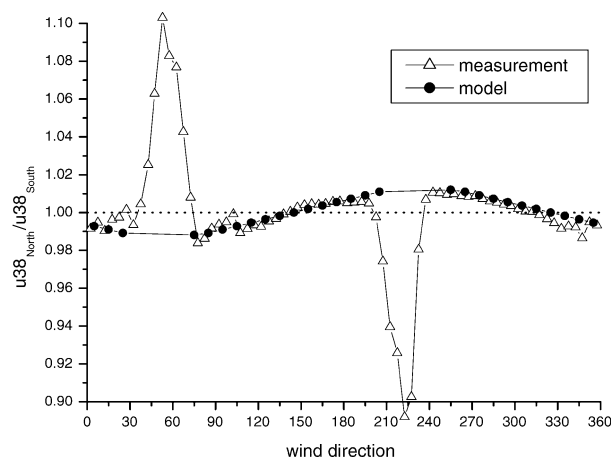


FIG. 8. Triangles: binned ratios of wind speed measurements at 38 m; circles: model results assuming flow distortion linear away from tower wake influence (see also Fig. 9). Data are from the Vindeby measurement program.

m s^{-1} ($0.0011 \text{ m s}^{-1} \text{ m}^{-1}$). The mean decrease of friction velocity with height, $7.1 \times 10^{-4} \text{ m s}^{-1}$ per meter of height difference from Eq. (13), is consistent with the data for both height differences. The average measured value has been used to derive the friction velocity at the surface from friction velocities derived at different heights from sonic and cup anemometer measurements.

2) CORRECTION OF WIND SPEEDS FOR FLOW DISTORTION OF THE MEASUREMENT MAST

At the Rødsand measurement mast, all cup anemometers as well as the sonic anemometer are mounted on booms pointing in the same direction $\sim 265^\circ$. Flow distortion from the measurement mast and the mounting of the instruments lead to measurement errors. They are obviously very large for situations with direct mast shade, and such records (wind directions $85^\circ \pm 35^\circ$) were omitted.

For other wind directions, a linear correction model was used, which was developed by Højstrup (1999) from measurements at a similar mast at the Vindeby site. In order to investigate the effects of flow distortion from the tower at the Vindeby site, anemometers were mounted on opposite sides of the mast at three different levels for a period of seven months. A triangular lattice measurement mast was used with a tower side length of 1.21 m and a boom length (measured from the nearest corner of the tower) of 2.51 m at 7-m height, leading to a ratio of boom length to tower side of approximately 2. At 20- and 38-m height it was about 2.5 and 4, respectively, with a tower side length of 0.95 and 0.60 m and a boom length of 2.40 and 2.32 m, respectively. The boom directions were 50° and 230° .

Taking the ratio of wind speeds on opposite sides of the tower, averaging in direction bins, a similar picture for all three heights (see Fig. 8 where only the highest

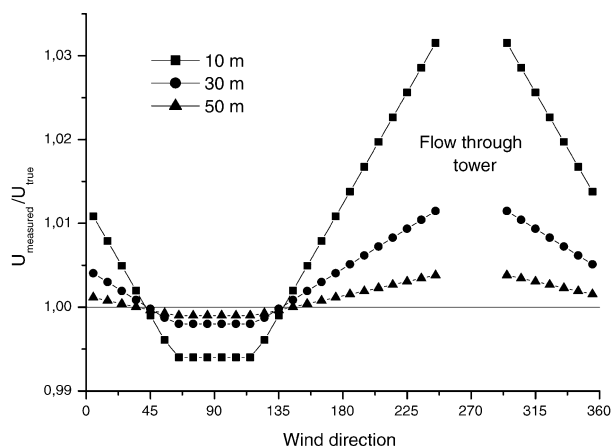


FIG. 9. Correction for tower flow distortion of wind speed at Rødsand as a function of wind direction with the model by Højstrup (1999). Note that the correction is positive on average and that the correction diminishes for increasing boom length to tower side ratio.

height is shown) can be seen. Also in Fig. 8 the result of a simple model (Højstrup 1999) is shown, assuming that the tower-induced flow distortion is linear in wind direction away from the sectors directly influenced by the wake of the tower. From Fig. 8 it is noted that the simple linear model works well outside of the sectors where one of the anemometers is in the wake of the mast and the other anemometer. For the three heights at Rødsand, correction factors of 1.033/0.994 (increase/decrease), 1.012/0.998, and 1.004/0.999 for the three heights 10, 30, and 50 m, respectively, are used for all wind speeds. Factors for the 50-m height are also used for the sonic anemometer mean wind speed and friction velocity. These are illustrated in Fig. 9 for all three heights.

Flow distortion of the wind speed standard deviation and the friction velocity is assumed to be similar to that of the mean wind speed, and the same correction factors are used for a simple correction. This approach is compared with measurements at Vindeby in Fig. 10. Ratios of wind speed standard deviations of the two anemometers are shown, similar to Fig. 8. A reasonable agreement between model and measurement is found.

3) TRANSFORMATION OF WIND SPEEDS TO WATER-FOLLOWING COORDINATES

For the interaction of wind with waves the relevant wind speed is the difference between air and water movement. Wind measurements made from fixed structures, like the measurement mast at Rødsand, therefore need to be corrected for the water current. At Rødsand, the water current is measured at a mean water depth of 2.4 m. Differences between the current at this depth and the surface current have been neglected, and all mean wind speeds measured at the mast have been transformed to refer to the moving reference frame of the water surface.

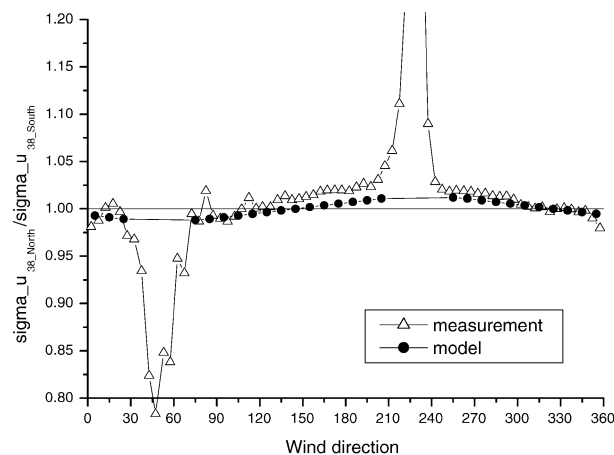


FIG. 10. Triangles: binned ratios of measurements of wind speed standard deviations at 38 m; circles: model results assuming flow distortion linear away from tower wake influence. Data are from the Vindeby measurement program.

At Rødsand currents are generally slow, usually below 0.4 m s^{-1} , and only on some occasions reach values up to 0.65 m s^{-1} . Differences in wind speed due to the transformation are for 93% of the records below 2% and for 99% below 5%.

e. Data selection

The first step in data selection is the rejection of data from nonstationary situations, that is, ones in which the ambient conditions change too much during the 30 minutes of the record under investigation. For the most important quantities the change in time is computed for a time period from 30 min before to 30 min after the averaging period of the record. Time periods with large gradients are rejected. This was done for wave phase speed, 10-m wind speed, friction velocity, and wind direction. Gradients of not more than $20\% \text{ h}^{-1}$ were allowed for wave phase speed and wind speed, 30% for friction velocity, and 40° for wind direction. Because of this limitation, 83% of all measured records were rejected.

The second step is to reject measurements for which the derived measured quantities cannot be calculated. This is the case if the measurement height of the sonic anemometer of about 45 m is above the surface layer. This can lead to friction velocity measurements that cannot be transformed to the surface value. As a simple approximation, the height of the surface layer can be estimated as 10% of the boundary layer height z_h , which is estimated by Tennekes (1982) as

$$z_h = 0.25 \frac{u_{*s}}{f_c}. \quad (14)$$

Using this expression, it is found that the surface layer might be shallower than 45 m if u_{*s} is smaller than about 0.2 m s^{-1} . Such measurements have been rejected.

The third step is to select only measurements where the conditions required by the theory under investigation are fulfilled. A simple power-law relationship between sea surface roughness and wave age cannot be expected to exist for situations in which other physical quantities play an important role, which are not represented in the power law. This is the case for situations 1) with non-neutral atmospheric stability, 2) with shallow-water effects influencing the wave field (apart from the influence of depth on c_p), 3) with a wave field that is not in local equilibrium with the wind, and 4) with flow that is not aerodynamically rough.

The condition of neutral atmospheric stratification is satisfied by correcting the measured wind speed for the influence of stability as described earlier. In addition, this correction is limited to a maximum of 3% correction in u_{10m} , and data with larger deviations from neutral stability are omitted. This leads to limits of $-0.5 < z/L < +0.3$ (with $z = 50 \text{ m}$).

The effect of water depth on the Charnock parameter is to some extent included in the wave age dependency since the wave phase speed c_p is changing with water depth. However, for even shallower water other effects, like enhanced whitecapping, will become important and are expected to have an influence on the Charnock parameter, which cannot be described by wave age alone. To avoid such cases, data with wave phase speed c_p (derived from the measurement) of less than 90% of the corresponding values for deep water waves are rejected.

The condition of locally generated wind waves is satisfied by selecting cases where the wave spectrum is single peaked. Furthermore, cases with a bandwidth close to that of the fitted JONSWAP spectrum are chosen. Records with a bandwidth of more than 0.25 are rejected (see Fig. 4).

For aerodynamically smooth flow the functional relation between the Charnock parameter and inverse wave age is expected to break down since the Charnock parameter may become dependent on the flow roughness Reynolds number. Therefore the analysis has to be confined to wave ages where smooth flow has no influence. In section 5b two approaches to ensure this are discussed. After Donelan (1990) the flow is rough if $u_* > 0.1 \text{ m s}^{-1}$, which is automatically fulfilled because of the selection for a minimum surface layer height (see above). The Toba et al. (1990) criterion of $R > R_{cr} = 2.3$ leads to a limit of inverse wave age of 0.05 for the Rødsand data (see discussion in section 5b). Rather than selecting data for this limit, it is indicated in the appropriate plots and data with inverse wave age below it should be treated with caution.

Four hundred and one (401) records (7% of the total number of records) are left in the final dataset.

3. Observed trend in sea roughness

a. Trend of sea roughness with wave age

Figure 11 gives an overview of the data. The Charnock parameter is plotted versus inverse wave age for

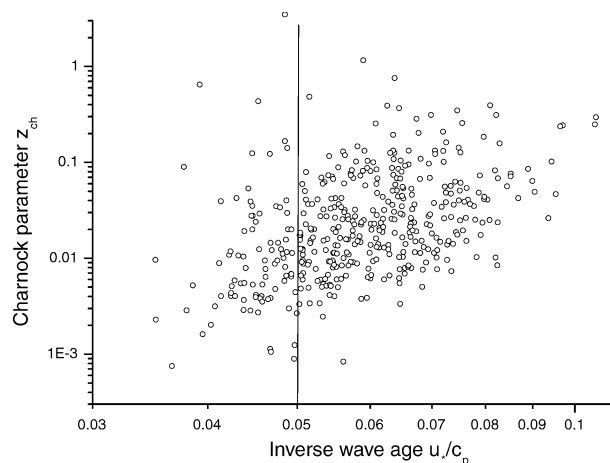


FIG. 11. The Charnock parameter vs inverse wave age from Rødsand data.

all half-hourly records. A bin-averaging method is used for trend investigation. First the data are sorted for the value of the inverse wave age in bins; the bin width is 0.01. Afterward, averages of u_{10m} , u_* , and u_*/c_p are calculated for the records in each bin. The bin values of z_{ch} are derived from the averaged parameters for each bin (see section 5 for a discussion of the bin-averaging method). The standard errors of u_{10m} and u_* have been used to estimate a standard error of the bin value of z_{ch} . Figure 12 shows a comparison of the bin values with the wave-age-dependent relation for the Charnock parameter from JHVL. Bearing in mind the measurement uncertainties, the agreement is good. However, from the error bars it can be seen that the scatter in the data is too large to allow a quantification of the parameters in a power law. This can only be done by using a dataset with a larger wave age variation as shown in section 3d.

Only one bin value is available for inverse wave ages

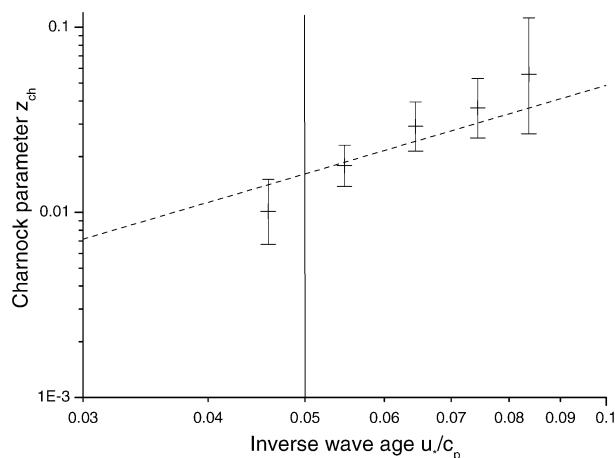


FIG. 12. The Charnock parameter vs inverse wave age from Rødsand data; bin values with respect to wave age are shown with their standard errors in comparison with the empirical fit of JHVL.

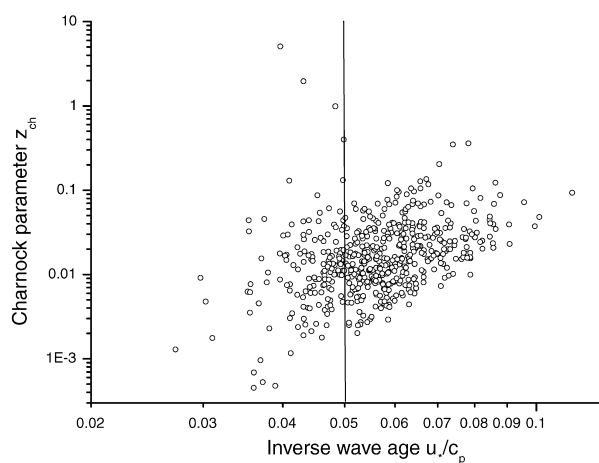


FIG. 13. The Charnock parameter vs inverse wave age from Rødsand data with friction velocity derived from cup anemometer measurement.

below the flow roughness limit of 0.05, that is, in the range where the trend might be influenced by smooth flow after the Toba et al. (1990) criterion. The value does not show a significant deviation from the observed general trend.

b. Trend obtained from cup anemometer measurements

With a sonic anemometer the wind stress can be measured using the well-established eddy-correlation method. Omnidirectional sonic anemometers such as the one used at Rødsand are, however, susceptible to flow distortion errors, especially in the vertical wind speed component and, therefore, in the friction velocity. Flow distortion errors are by their nature wind direction dependent. A concern is therefore that they coincide with a wind-direction-dependent variation of wave age values due to different fetch lengths. This could distort or even cause the observed trend of sea surface roughness with wave age.

To rule out this concern, the friction velocity has also been derived by an alternative indirect method from cup anemometer measurements [see section 2c(1)]. The method requires that the marine boundary layer is in an equilibrium condition. This can be assumed for the data with near-neutral stratification and nearly stationary conditions used in this analysis. This method is expected to be less accurate than the direct eddy-correlation method, but has the advantage of ruling out wind-direction-dependent flow distortion errors.

Data have been analyzed as before, but with the friction velocity derived from the cup anemometer at 10-m height instead of the sonic anemometer. No selection has been made for low friction velocities since the measurement height of 10 m can be expected to always be in the surface layer. The resulting data are shown in Fig. 13 as the Charnock parameter versus inverse wave age.

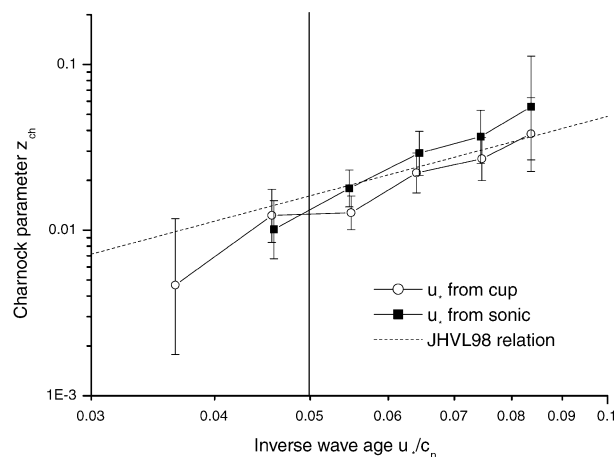


FIG. 14. The Charnock parameter vs inverse wave age from Rødsand data with friction velocity derived from cup and sonic anemometer measurements; bin values with respect to wave age are shown with their standard errors in comparison with the empirical fit of JHVL.

The data have been bin averaged as described in section 3a. Figure 14 shows the result in comparison with the result obtained from the sonic anemometer and the relation proposed by JHVL. The result from the analysis of the cup anemometer data supports the trend found from the sonic anemometer.

c. Trend obtained for different fetch lengths

The measurement location experiences fetches in a wide range from 10 to more than 100 km (see Fig. 1). To test a possible dependence of the relation between the Charnock parameter and inverse wave age, four wind direction sectors with approximately uniform fetches have been selected (Table 2).

This requires selection of the data for narrow wind direction sectors. The wind-direction-dependent flow distortion error of the sonic anemometer would in this case distort the results since the Charnock parameter is very sensitive to a bias in friction velocity (an error of 8% in friction velocity causes a doubling of the Charnock parameter). Therefore the friction velocity derived from the cup anemometer has been used [see section 2c(1)]. The data have been analyzed as described in section 3b.

Bin values of the Charnock parameter are plotted against inverse wave age for each wind direction sector (see Fig. 15). The trend of increasing Charnock parameter with inverse wave age is generally confirmed, although with larger variations. These are caused by the low number of measurement data available in each wind direction sector (see Table 2). A systematic variation of the relation with fetch length is not visible; that is, a dependence of the coefficients of the power-law relation between Charnock parameter and inverse wave age on fetch length cannot be found.

TABLE 2. Selected wind direction sectors with approximately uniform fetch.

Wind direction (°)	Sector	Fetch (km)	No. of records
200–230	Lübecker Bucht	60–90	102
240–260	Fehmarn	30–40	49
270–290	Femerbelt	>100	77
300–350	Lolland	10–20	50

d. Trend obtained for an aggregated dataset

The range of inverse wave age available at one measurement site is relatively small (in the Rødsand dataset typically $0.04 < u_*/c_p < 0.09$). This, together with the considerable scatter in the data, makes the determination of the parameters of a power-law relation unreliable. Following JHVL, measurement data from different locations and with a wide range of wave age values have therefore been combined in an aggregated dataset. Data compiled in Donelan et al. (1993) have been used.

For each dataset the median values of the Charnock parameter and inverse wave age have been plotted (Fig. 16). The median has been used as an approximation to the bin values from averaged measured quantities, since the measured quantities were not available individually. It can be seen that the result for the Rødsand measurement is close to the trend line proposed by JHVL.

A comparison with other proposed trend lines in the literature (Toba et al. 1990; Drennan et al. 2003; Maat et al. 1991; Monbaliu 1994; Smith et al. 1992) is made in Fig. 17. It can be seen that a wide range of coefficients has been found for the power-law relation $z_{ch} = A(u_*/c_p)^B$ (see Table 3). Some possible reasons for these differences are discussed in the following section.

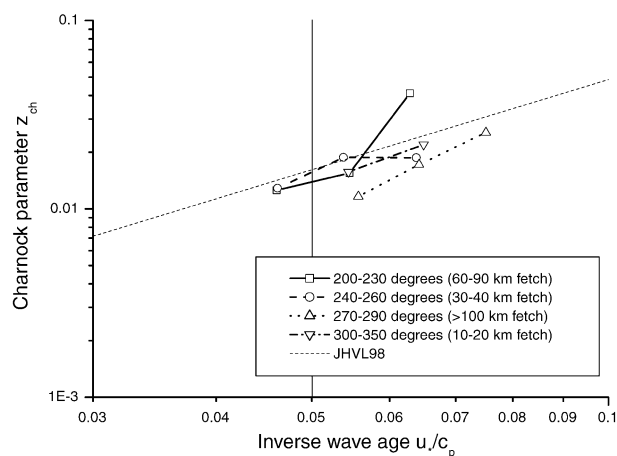


FIG. 15. The Charnock parameter vs inverse wave age from Rødsand measurement bin averaged with respect to wave age; data from four wind direction sectors with different fetches are shown together with the empirical fit of JHVL.

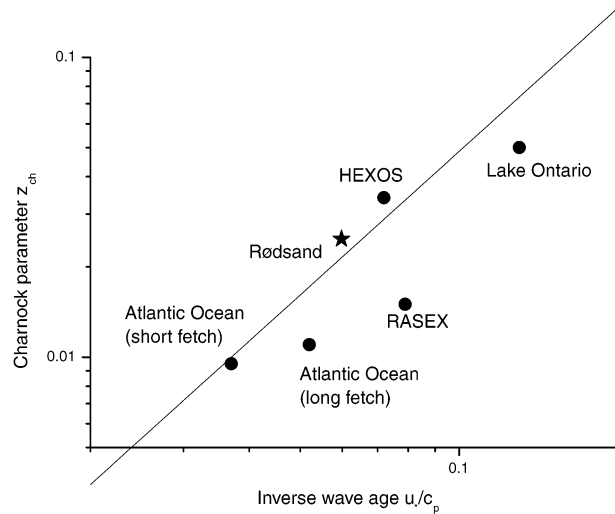


FIG. 16. Scatterplot of the averaged Charnock parameter vs inverse wave age for several datasets and comparison with the empirical fit of JHVL.

4. Influence of self-correlation

In Hicks (1981) a numerical method is described for investigating the functional relationship introduced by self-correlation. A functional relation is derived from an artificial random “dataset” of unrelated values for the input parameters in the analysis. The functional relationship found will solely be a result of the correlation introduced in the analysis. The wave phase speed c_p is the only wave parameter in the relation of a wave-age-

TABLE 3. Parameter values proposed for the power-law relation

$$z_{ch} = A (u_*/c_p)^B.$$

Source	A	B
Toba et al. (1990)	0.02	-0.5
Maat et al. (1991)	0.8	1
Smith et al. (1992)	0.48	1
Monbaliu (1994)	2.87	1.69
JHVL	1.89	1.59
Drennan et al. (2003)	1.7	1.7

dependent Charnock parameter. The question is whether the introduction of the wave phase speed leads to a relation between the Charnock parameter and wave age that has physical meaning and is not a mere result of self-correlation.

For this purpose an artificial dataset has been produced in which the measured values of wave phase speeds are replaced by random numbers. Instead of a uniformly distributed probability of the values as proposed by Hicks (1981), the probability distribution is chosen to follow those of the measured dataset (Fig. 18c). This is done by randomly redistributing the measured data of wave phase speed within the dataset. To increase the data volume and improve “randomness” the measured dataset has been repeated several times. For friction velocity and neutral 10-m wind speed the actual measurement values are used without change. Figures 18a and 18b show their probability distributions in the Rødsand dataset.

Figure 19 shows the Charnock parameter versus inverse wave age for the random data. This can be com-

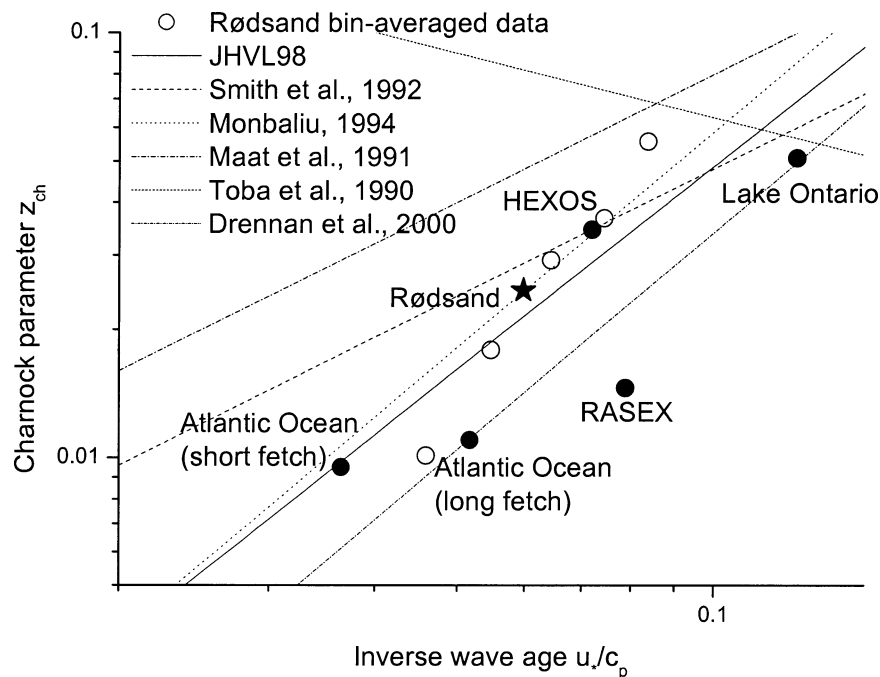


FIG. 17. Comparison of the averaged Charnock parameter vs inverse wave age for several datasets with proposed empirical relations.

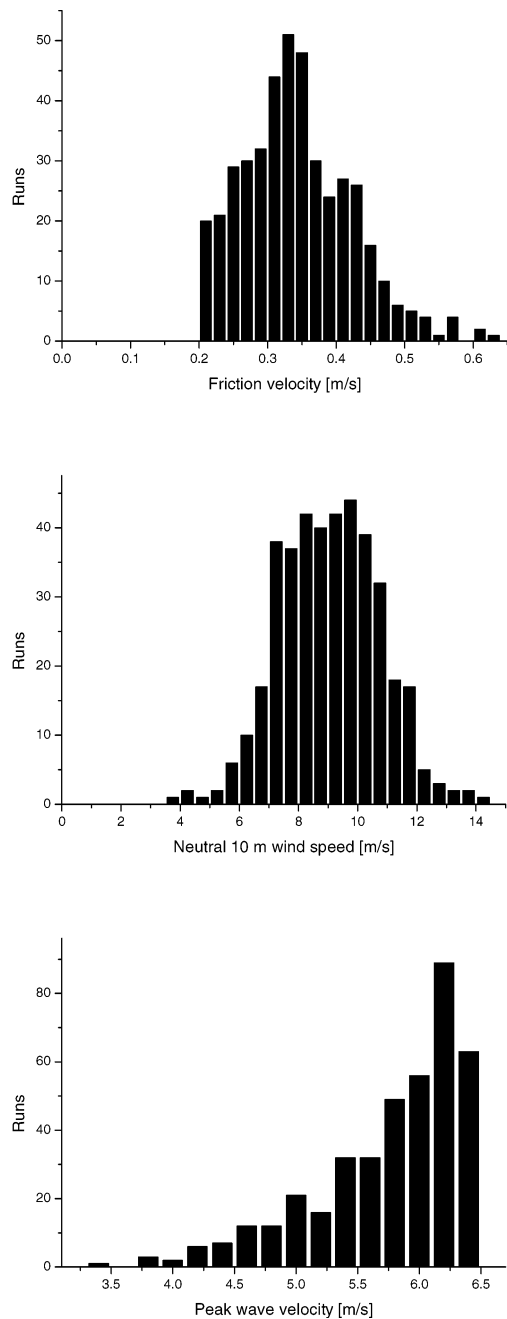


FIG. 18. Probability distributions of u_* , u_{10n} , and c_p in the measured Rødsand data.

pared with the measured data from Rødsand shown in Fig. 11. Clearly the data points from the random data show larger spread. However, a trend of increasing Charnock parameter for increasing inverse wave age can be found in both figures. This is clearly an undesired influence of the common scaling variable u_* .

The random data have subsequently been analyzed in the same way as the real data (see the previous section). The data have been sorted according to wave age bins;

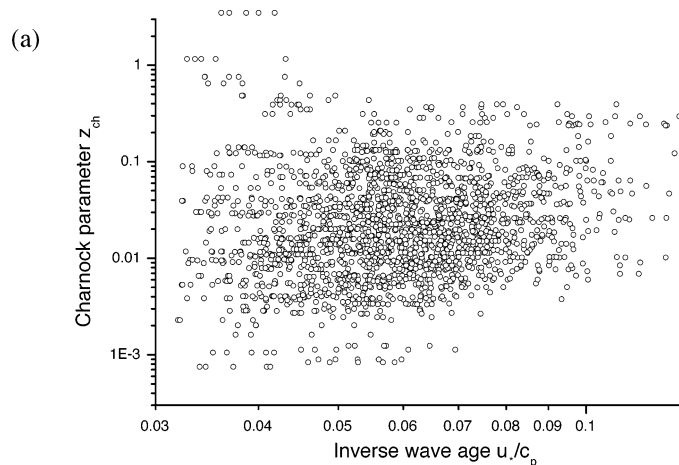


FIG. 19. The Charnock parameter vs wave age from simulated random “data.”

the input quantities u_{10n} , u_* , and c_p have been averaged for each bin; and the bin values of the derived quantities z_{ch} and wave age have been found from these averaged values. Figure 20 shows the resulting bin values of the random data in comparison with those of the measured data and the trend line from JHVL. It is obvious that all three trend lines increase for increasing inverse wave age. The trend line of the random dataset is the result of self-correlation of the friction velocity u_* . Its difference from the trend line of the measured data is the result of the physical dependency of the Charnock parameter on the wave phase speed c_p . Both trends appear to be different, with the one for random data showing a smaller slope. However, uncertainties in the measured data, as illustrated by the error bars, are too large to allow the difference in trends to be conclusive; that is, because of self-correlation not even the existence of a physical dependency between the Charnock constant and wave age can be deduced from this dataset. This

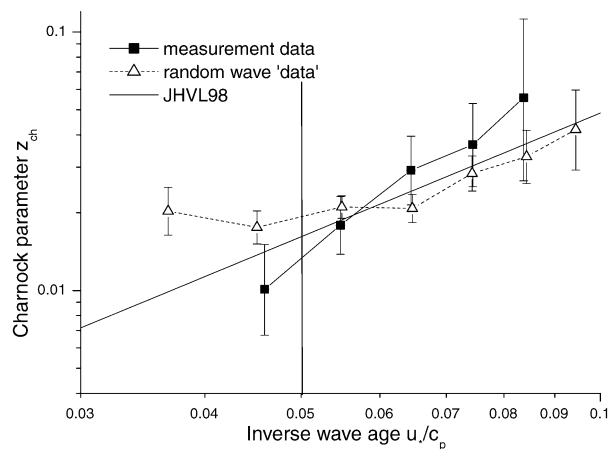


FIG. 20. Wave age bin values of the Charnock parameter vs inverse wave age from the Rødsand measurement and the simulated random data; also shown is the JHVL relation.

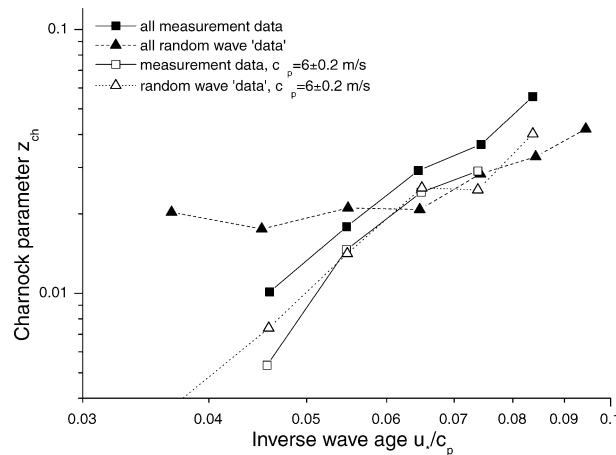


FIG. 21. Comparison of wave age dependency of the Charnock parameter for all data and a data subset with wave phase speed $c_p = 6 \pm 0.2 \text{ m s}^{-1}$; shown are results from the Rødsand measurement and simulated random datasets.

confirms the conclusion of JHVL that a trend that is not severely influenced by self-correlation can only be found when an aggregated dataset is used. The range of wave age values has to be large enough to allow a statistically significant separation between the observed trend line and the trend line obtained without wave information.

Ideally, the self-correlation should be investigated for the aggregated dataset used in section 3d. The measured quantities of these datasets were not available. Instead, a smaller subset of the Rødsand data is used to investigate the effect of different datasets on self-correlation. For this data subset, only records with a nearly constant wave phase speed c_p of $6 \pm 0.2 \text{ m s}^{-1}$ have been selected. The analysis of the data as well as the compilation and analysis of a simulated random dataset has been repeated and compared with the result of all data (Fig. 21). The Charnock parameters found from the subset of measured data with nearly constant c_p are slightly lower, while the steepness of the trend relation remains largely unchanged. This is different for the randomized data. Obviously, randomizing c_p in a data subset where it is nearly constant does not lead to significant changes, and the trend of the Charnock parameter with inverse wave age for the randomized data is the same as for the measured data; that is, the relation is completely determined by self-correlation. Using all measured data, that is, the whole range of c_p values available at this particular site (see Fig. 18), the difference between measured and randomized data in the trends of the Charnock parameter versus inverse wave age becomes larger. However, as mentioned above, the range of c_p values is not wide enough to allow a statistically significant separation of both trends for the Rødsand dataset. For a dataset with a very wide range of c_p values, which could be obtained by aggregating data from different sites, it can be expected that the trends of measured and randomized

data are more separated. In this way the effect of self-correlation could be separated from the physical dependency between the Charnock constant and wave age.

5. Discussion of the analysis method

a. Bin averaging

For the dependence of the Charnock parameter on inverse wave age a power-law relation is assumed. The coefficients of the relation have to be found empirically by a fit to measured data. A problem arises if the data show a large statistical spread and one of the scaling groups does not follow a normal probability distribution.

Data for measured Charnock parameters have a large spread, mainly due to the sampling variability in u_* . Also, the Charnock parameter depends on physical quantities of u_* and u_{10m} in a highly nonlinear way [see Eq. (7)]. Therefore it cannot simply be averaged, and a fit based on an rms error of z_{ch} does not seem suitable. A simple example: assuming three records with u_{10m} of 10 m s^{-1} and u_* of 0.2, 0.3, and 0.4 m s^{-1} , the z_{ch} values are calculated to 0.000 005, 0.001, and 0.03. The average of the z_{ch} values is 0.01. If instead the physical measured quantities are averaged and z_{ch} is calculated from the average u_{10m} and u_* values, the average z_{ch} is 0.001, that is, an order of magnitude smaller.

To avoid these problems, a bin-averaging method is used instead of a direct fit or an averaging of z_{ch} . The procedure generally consists of two steps. First the data are sorted for the value of one parameter (sorting parameter) into bins. Afterward one or several parameters are averaged over all records in each bin (averaged parameters) and derived quantities are calculated from these (bin values). In the resulting bin values the large statistical spread has vanished and a linear fit can be made to determine the coefficients of the power-law relation. For the determination of a power-law relation between the Charnock parameter and inverse wave age, the inverse wave age is used as the sorting parameter. The averaged parameters are the measured quantities u_* , u_{10m} , and c_p . The Charnock parameter is then calculated from these averaged values for each bin. As an estimate of the measurement uncertainty, standard errors of z_{ch} are calculated from the standard errors of the averaged quantities.

Figure 22 shows the difference between the fits of a power-law relation to the measured Charnock parameters and the bin values. The large difference is obvious. Also shown is the result of a fit to the logarithm of the measured Charnock parameter $\log_{10}(z_{ch})$. It can be seen that this is a good approximation to the bin-averaging method.

In the previous section it was shown that the trend of the Charnock parameter with inverse wave age is influenced, or even determined by, the self-correlation due to the variability in u_* , depending on the range of the u_* and c_p values in the dataset. Since this self-

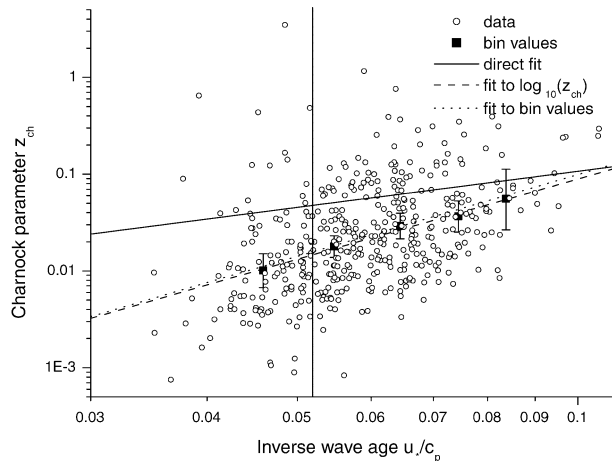


FIG. 22. Comparison of methods to fit a power-law relation between the Charnock parameter and inverse wave age to measured data.

correlation is part of the relation found from the measured data, it will also differ for different datasets. This partly explains the differences found from different datasets for the coefficients of the power-law relation. The effect of different datasets on the relation found is shown again in Fig. 23 for three different wind speed intervals. The data have been sorted according to wind speed and inverse wave age in a two-dimensional bin averaging. The small squares show the bin values of the Charnock parameter versus inverse wave age for a certain wind speed and inverse wave age interval. It is found that the trend relation is steeper for a narrow wind speed interval because of the dominating influence of self-correlation in u_* . Figure 23 also shows how the choice of the sorting parameter can influence the result of the trend investigation. The large squares are the bin values for the three wind speed intervals without sorting for inverse wave age. The different sorting parameter, in this case wind speed, leads to a different apparent trend of the Charnock parameter with inverse wave age.

b. Rough flow condition

One of the conditions for the dependence of sea surface roughness on wave age alone is that the airflow must be rough turbulent (see JHVL). If this condition is not satisfied, it can be expected that the sea surface roughness would also depend on the roughness Reynolds number of the flow.

JHVL and others (e.g., Drennan et al. 2003) follow Toba et al. (1990) in defining a limiting roughness Reynolds number $R_{cr} = u_* z_0 / \nu$ (ν is kinematic viscosity) for fully rough flow of 2.3. Since the value is important for the selection of data, an attempt is made to uncover its origins in the literature. Toba et al. (1990) quote Schlichting (1979), who defines aerodynamically fully rough flow by

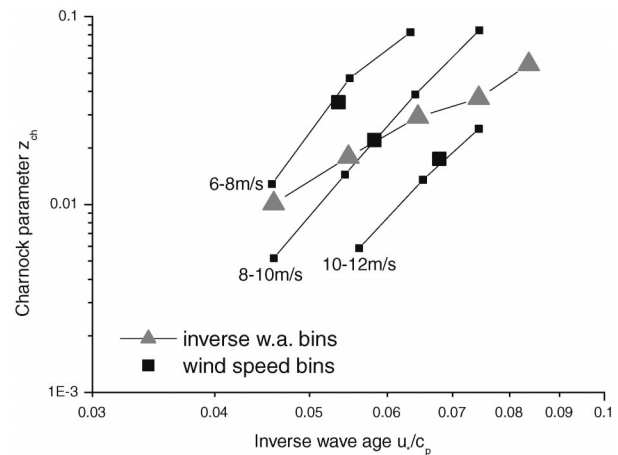


FIG. 23. The Charnock parameter vs wave age from Rødsand measurements; bin values from bin averaging with respect to inverse wave age (large triangles) and with respect to the neutral wind speed at 10-m height (large squares) are shown as well as bin values after the data were sorted and bin averaged both in wind speed and inverse wave age bins (small squares).

$$\frac{u_* k_s}{\nu} > 70; \quad (15)$$

here k_s is the sand grain size used in experiments in rough pipes by Nikuradse (1933). For other flows this is related to the roughness parameter k by the formula empirically found by Schlichting (1936):

$$5.75 \log_{10} \left(\frac{k_s}{k} \right) = 8.5 - B. \quad (16)$$

Concerning the flow of natural winds over the surface of the earth, Schlichting reports findings from Paeschke (1937), who found $B = 5$ when the physical height of the vegetation is used as roughness parameter k . This leads to the relation $k_s = 4k$ between Nikuradse's sand grain size k_s and the roughness parameter k . The logarithmic profile used by Schlichting,

$$\frac{u}{u_*} = 2.5 \ln \left(\frac{z}{k} \right) + B, \quad (17)$$

can be used to relate his roughness parameter k to the surface roughness length z_0 . Inserting the result, $k = 7.4z_0$, and $k_s = 4k$ into Eq. (17) leads to the limiting roughness Reynolds number used by JHVL and Toba et al. (1990):

$$R_{cr} = \frac{u_* z_0}{\nu} = 2.3. \quad (18)$$

Kitaigorodskii (1970) takes a similar approach, also based on the measurements of Nikuradse (1933), and finds a similar limiting value of 3.0. The many assumptions about the similar behavior of flow through pipes and in the atmosphere and about the similar effects

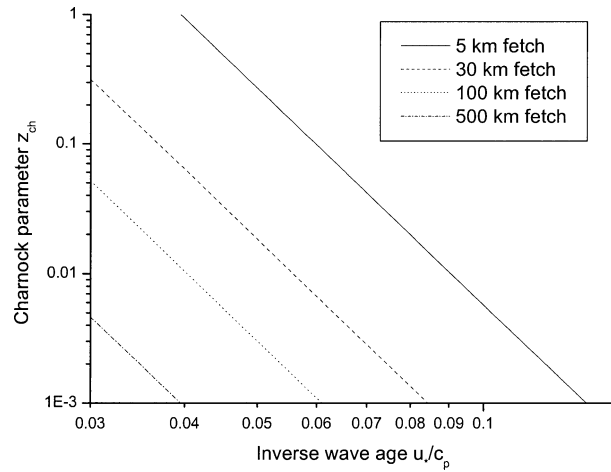


FIG. 24. Sensitivity of the roughness flow criterion of JHVL with fetch on a plot of the Charnock parameter vs inverse wave age ($R_{cr} = 2.3$); based on Eq. (21).

of sand, vegetation, and waves suggest that these values should be used with caution.

In the following it is shown that the application of the roughness Reynolds number as a roughness criterion in a dataset with large scatter can lead to a misleading impression about the overall trend in a plot of z_{ch} versus u_*/c_p depending on the effective fetch of the site. This is caused by the large scatter of the measured sea surface roughness, which enters into the selection criterion as part of the flow roughness.

The rough flow condition can be written in terms of the Charnock parameter as

$$z_{ch} > R_{cr} g \nu u_*^{-3}, \quad (19)$$

where $R_{cr} = z_0 u_*/\nu$ is the critical flow roughness for rough, turbulent flow. For growing wind waves in fetch-limited cases in deep water, Kahma and Calkoen (1994) obtained the following relationship:

$$\frac{u_*}{c_p} = 3.08(gX)^{-0.27} u_*^{0.54}. \quad (20)$$

Equations (19) and (20) can be combined to give

$$z_{ch} > 520.4 R_{cr} g \nu (gX)^{-1.5} \left(\frac{u_*}{c_p} \right)^{-5.56}. \quad (21)$$

Equation (21) is the roughness flow condition expressed in terms of the dimensionless sea roughness (Charnock parameter), inverse wave age, and fetch. In a plot of z_{ch} versus u_*/c_p , this condition filters out all data points below the line given by Eq. (21). The number of data points filtered out depends on the effective fetch at the site. This is illustrated in Fig. 24 ($R_{cr} = 2.3$, $g = 9.81 \text{ m s}^{-2}$, $\nu = 1.461 \times 10^{-5} \text{ m}^2 \text{ s}^{-1}$), which shows the limiting line of Eq. (21) for different fetch lengths. It can be seen that for typical ranges of z_{ch} and u_*/c_p and short to moderate fetch lengths (<50 km) a large amount of data is filtered out, while a relatively small amount of data is filtered out for the longest fetch lengths (>500 km).

Figure 25 shows the Rødsand data segregated according to the flow roughness number. A trend of increasing Charnock parameter with inverse wave age can be seen, although with a large scatter in the data. Figure 25 also shows the calculated Reynolds criterion line

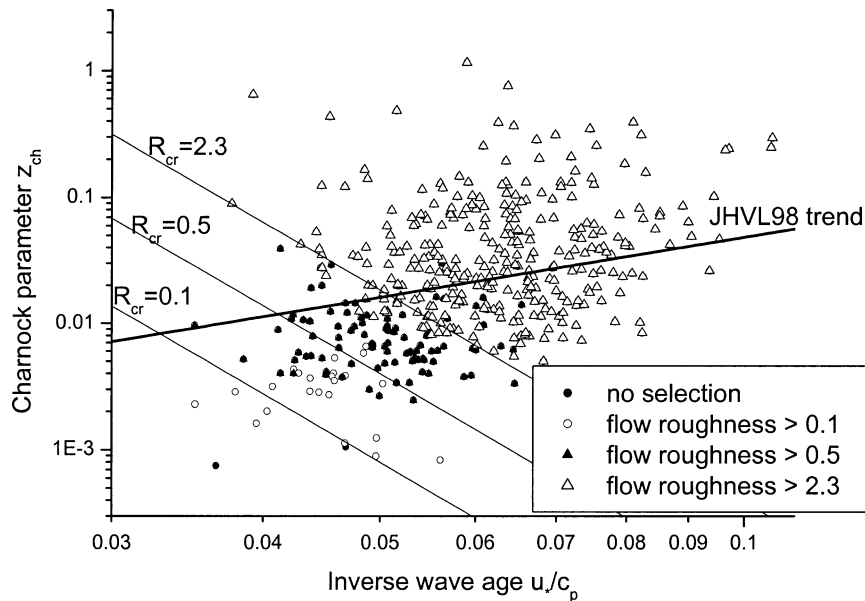


FIG. 25. The Charnock parameter vs inverse wave age from Rødsand data segregated according to flow roughness; also shown are the limiting lines of Eq. (21) for an effective fetch of 30 km and $R_{cr} = 2.3$, 0.5, and 0.1.

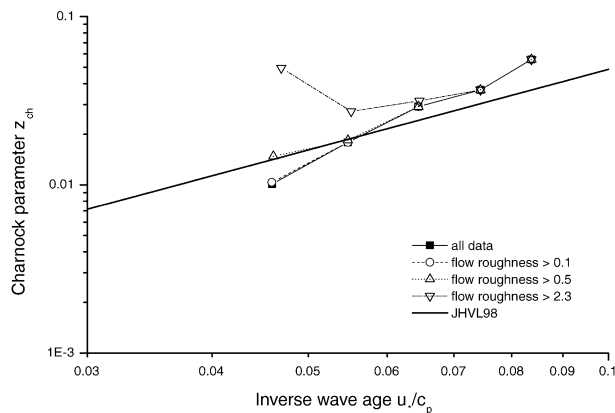


FIG. 26. The Charnock parameter vs inverse wave age for different flow roughness selection criteria.

using Eq. (21). It is observed that this corresponds closely to the data when an effective fetch of 30 km is used for the site. For this particular case, the average effective fetch was obtained using Eq. (20) and the measured values of c_p and u_* . Note that the effective fetch is not the same as the physical fetch, since the former also includes the influence of wind duration and water depth; Eq. (20) is only valid for deep water and waves that are not duration limited.

Applying this condition as a selection criterion to the data before bin averaging leads to problems. This is demonstrated in Fig. 26, where the influence of the choice of flow roughness limit on the relation of the Charnock parameter with wave age is shown. The data have been selected for different choices of the flow roughness limit and thereafter bin averaged. It can be seen that the relation between the Charnock parameter and inverse wave age at small inverse wave ages changes drastically for different flow roughness criteria. This shows that for short to moderate fetch lengths, the scatter above the roughness criterion line can present itself as a trend of decreasing z_{ch} with increasing inverse wave age; that is, it can lead to a misleading impression about the overall trend in a plot of z_{ch} versus u_*/c_p . This is probably the cause of the similar apparent trend in the RASEX data as reported by JHVL. It can also be seen that the obtained trend—apart from the mentioned distortion—does not depend on the value used for the selection criterion for the flow roughness.

Drennan et al. (2003) report a different behavior for data with a low inverse wave age, which led them to reject data with $u_*/c_p < 0.05$. They attributed this to a difference between growing and fully developed waves. However, the data selection for rough flow is probably another possible explanation.

If it is assumed that the relation between z_{ch} and u_*/c_p is real and the scatter in the data around it is due to measurement variability, the criterion for flow roughness should be applied to the physical relation rather than the scattered data including measurement vari-

ability. In Fig. 25 it can be seen that the limiting line for the roughness Reynolds number for an effective fetch of 30 km and $R_{cr} = 2.3$ crosses the JHVL trend line at an inverse wave age of about 0.05. This criterion should therefore be used by rejecting data with lower inverse wave ages. In this way the distortion of the result due to application of a selection criterion to a scattered dataset is avoided.

An approach different from that used by Toba et al. (1990) and Kitaigorodskii (1970) is proposed by Donelan (1990), who summarizes open-ocean experiments from Smith (1980) and Large and Pond (1981). He distinguishes only between smooth and rough flow and used the friction velocity as criterion for flow roughness:

$$z_0 = 0.11 \frac{\nu}{u_*}$$

$$\text{for } u_* < 2(\nu g)^{1/3} = 0.1 \text{ m s}^{-1} \quad (\text{smooth flow}) \quad (22)$$

and

$$z_0 = 0.014 \frac{u_*^2}{g}$$

$$\text{for } u_* > 2(\nu g)^{1/3} = 0.1 \text{ m s}^{-1} \quad (\text{rough flow}). \quad (23)$$

The limit for u_* is the value where the sea surface roughness for smooth and rough flow are equal. For the Rødsand data this criterion is automatically fulfilled since data with $u_* < 0.2 \text{ m s}^{-1}$ have already been rejected to ensure that the sonic anemometer is in the surface layer (see section 2e).

6. Conclusions

New simultaneously measured wind and wave data from the field measurement program at Rødsand in the Danish Baltic Sea are presented. These data have been used to test the wave age dependence of the Charnock parameter (or dimensionless sea surface roughness). A general trend of increasing sea roughness with inverse wave age is obtained that agrees with the trend found in JHVL and similar parameterizations.

However, by analyzing a simulated dataset of randomly generated wave “data” it was shown that self-correlation severely influences the observed relation between the Charnock parameter and wave age. Uncertainties in the measured data are too large to allow the difference in trends between real and simulated random data to be conclusive. This means that, with the Rødsand dataset alone, not even the existence of a physical dependency between the Charnock parameter and wave age can be proven.

By using a small subset of the Rødsand data it was shown that for a dataset with a narrow range of c_p the trend lines of real and random data become almost identical. The larger the range in c_p values is, the less significant is the influence of self-correlation. In other words, the wave age variation needs to be caused by the variation in c_p , not by the spreading in u_* . We be-

lieve that for a dataset with a very large range of wave age values the influence of self-correlation and physical dependency can be separated. This supports the basic idea of JHVL—that a trend, which is not severely influenced by self-correlation, can only be found with an aggregated dataset where the range of wave phase speed values is large. Further research is needed here.

From this investigation it becomes clear that the dependence of the Charnock parameter on wave age is less pronounced than what could be expected without taking into account the influence of self-correlation. We therefore expect that, even if the physical nature of the trend can be shown with such an aggregated dataset, the improvement of the Charnock relation with a wave-age-dependent Charnock parameter is limited. Future research should also consider alternative approaches for the parameterization of the Charnock parameter, for example, with wave height or wave steepness.

In the literature, different coefficients for the power law between the Charnock parameter and wave age have been found for different datasets. Such differences can be expected since for different datasets—and hence different ranges of the quantities u_* and c_p —different self-correlation relations follow that lead to different coefficients in the power-law relation.

Additionally, it is shown that the roughness Reynolds number criterion often applied to select data with rough, turbulent flow can lead to a misleading impression about the trend in the data since the sea surface roughness is present in both the selection rule and in the quantity under investigation. This is believed to be the cause of the apparent trend of a decrease in the Charnock parameter with inverse wave age in the RASEX data as reported by JHVL. The importance of this distortion varies with the effective fetch length at the site. It is mainly important for short to medium fetch lengths. Two alternative methods used to ensure aerodynamically rough flow are discussed, which do not distort the relation. Instead of applying the roughness Reynolds number criterion to the (scattered) data it can be applied to the relationship found. This leads to a limiting inverse wave age, which in the case of the Rødsand data is $u_*/c_p > 0.05$. A different criterion for rough flow is the one of Donelan (1990), who finds a limit of $u_* > 0.1 \text{ m s}^{-1}$ for rough flow by equating the sea surface roughness estimated for rough and smooth flow.

A misleading trend can also be caused by the methods used to obtain the parameterization from the data. Investigation of the bin-averaging method showed that the choice of the sorting parameter in the bin-averaging analysis can lead to an inversion of the observed trend of the Charnock parameter with wave age.

To sum up, we conclude that the parameterization of the Charnock parameter as a function of wave age is fraught with many difficulties; hence, one must be cautious in using such a relationship, especially if derived from single-site measurements. Some of the difficulties include the influence of self-correlation, selective fil-

tering introduced by the roughness flow condition, and the usually large scatter in the Charnock parameter itself. Some of the differences found in the literature can probably be explained by these difficulties.

The Rødsand data show an increase of the Charnock parameter with inverse wave age in line with most literature results. While the existence of the trend seems clear, the significance of it is not. We find that the importance of the physical dependency in the Rødsand dataset is questioned by self-correlation effects, that is, that the relation is severely influenced by self-correlation. However, our results indicate that the self-correlation effects can be reduced by using a dataset with an equally strong variability of the different data entering into the regression procedure, as for example by aggregating datasets as in JHVL.

Acknowledgments. This research was funded by the Danish Technical Research Council (STVF) as part of the Wind-Wave Interaction in Coastal and Shallow Areas project. We gratefully acknowledge the financial support of the Rødsand measurement program by the following: European Union, JOULE program (JOU2-CT93-0325), Office of Naval Research (N00014-93-1-0360), and ELKRAFT. The work of one of the authors (BL) was partly funded by the European Commission through a Marie Curie Research Training Grant. Many thanks are given to Rebecca Barthelmie from Risø for managing the Rødsand field experiment since 1998. The technical support team at Risø and H. Kobbernagel of Sydfalster-El are acknowledged for their contribution to the data collection. The authors thank the reviewers for their important and useful comments, which led to a substantial improvement of the paper.

REFERENCES

- Charnock, H., 1955: Wind stress over a water surface. *Quart. J. Roy. Meteor. Soc.*, **81**, 639–640.
- Donelan, M. A., 1990: Air–sea interaction. *The Sea*, B. Le Mehauté and D. M. Hanes, Eds., Ocean Engineering Science, Vol. 9, John Wiley and Sons, 239–292.
- , F. W. Dobson, S. D. Smith, and R. J. Anderson, 1993: On the dependence of sea surface roughness on wave development. *J. Phys. Oceanogr.*, **23**, 2143–2149.
- Drennan, W. M., H. C. Graber, D. Hauser, and C. Quentin, 2003: On the wave age dependence of wind stress over pure wind seas. *J. Geophys. Res.*, **108** (C3), 8062, doi:10.1029/2000JC000715.
- Garratt, J. R., 1992: *The Atmospheric Boundary Layer*. Cambridge University Press, 316 pp.
- Geernaert, G. L., K. B. Katsaros, and K. Richter, 1986: Variation of the drag coefficient and its dependence on sea state. *J. Geophys. Res.*, **91**, 7667–7679.
- Hasselmann, K., and Coauthors, 1973: Measurements of wind-wave growth and swell decay during the Joint North Sea Wave Project (JONSWAP). *Dtsch. Hydrogr. Z. (Suppl.)*, **A12** (8), 1–95.
- Hicks, B. B., 1978: Some limitations of dimensional analysis and power laws. *Bound.-Layer Meteor.*, **14**, 567–569.
- , 1981: An examination of turbulence statistics in the surface boundary layer. *Bound.-Layer Meteor.*, **21**, 389–402.
- Højstrup, J., 1999: Vertical extrapolation of offshore wind profiles. *Wind Energy for the Next Millennium: Proc. European Wind*

- Energy Conf.*, Nice, France, European Wind Energy Association, 1220–1223.
- Hsu, S. A., 1974: A dynamic roughness equation and its application to wind stress determination at the air–sea interface. *J. Phys. Oceanogr.*, **4**, 116–120.
- Johnson, H. K., J. Højstrup, H. J. Vested, and S. E. Larsen, 1998: On the dependence of sea surface roughness on wind waves. *J. Phys. Oceanogr.*, **28**, 1702–1716.
- Kahma, K. K., and C. J. Calkoen, 1994: Growth curve observations. *Dynamics and Modelling of Ocean Waves*, G. J. Komen et al., Eds., Cambridge University Press, 174–182.
- Kitaigorodskii, S. A., 1970: *The Physics of Air–Sea Interaction*. Israel Program for Scientific Translations, 237 pp. (Translated from Russian by A. Baruch.)
- Lange, B., R. J. Barthelmie, and J. Højstrup, 2001: Description of the Rødsand field measurement. Risø National Laboratory Rep. Risø-R-1268, 59 pp. [Available from Risø National Laboratory, Bldg. 115, P.O. Box 49, DK-4000 Roskilde, Denmark; also available online at www.risoe.dk.]
- Large, W. G., and S. Pond, 1981: Open ocean momentum flux measurements in moderate to strong winds. *J. Phys. Oceanogr.*, **11**, 324–336.
- Maat, N., C. Kraan, and W. A. Oost, 1991: The roughness of wind waves. *Bound.-Layer Meteor.*, **54**, 89–103.
- Monbaliu, J., 1994: On the use of the Donelan wave spectral parameter as a measure for the roughness of wind waves. *Bound.-Layer Meteor.*, **67**, 277–291.
- Mortensen, N. G., and J. Højstrup, 1995: The solent sonic—Response and associated errors. Preprints, *Ninth Symp. on Meteorological Observations and Instrumentation*, Charlotte, NC, Amer. Meteor. Soc., 501–506.
- Nikuradse, J., 1933: Strömungsgesetze in rauen Röhren. *Forsch. Arb. Ing.-Wes.*, **361**, 1–22.
- Paeschke, W., 1937: Experimentelle Untersuchungen zum Rauheits- und Stabilitätsproblem in der bodennahen Luftschicht. Ph.D. dissertation, Universität Göttingen, 48 pp.
- Schlichting, H., 1936: Experimentelle Untersuchungen zum Rauheitsproblem. *Ing.-Arch.*, **7**, 1–34.
- , 1979: *Boundary-Layer Theory*. McGraw-Hill, 817 pp.
- Schotanus, P., F. T. M. Nieuwstadt, and H. A. R. De Bruin, 1983: Temperature measurement with a sonic anemometer and its application to heat and moisture fluxes. *Bound.-Layer Meteor.*, **26**, 81–93.
- Smith, S. D., 1980: Wind stress and heat flux over the open ocean in gale force winds. *J. Phys. Oceanogr.*, **10**, 709–726.
- , and Coauthors, 1992: Sea surface wind stress and drag coefficients: The HEXOS results. *Bound.-Layer Meteor.*, **60**, 109–142.
- Stull, R. B., 1988: *An Introduction to Boundary Layer Meteorology*. Kluwer Academic, 666 pp.
- Taylor, P. K., and M. J. Yelland, 2001: The dependence of sea surface roughness on the height and steepness of the waves. *J. Phys. Oceanogr.*, **31**, 572–590.
- Tennekes, H., 1982: Similarity relations, scaling laws and spectral dynamics. *Atmospheric Turbulence and Air Pollution Modelling*, F. T. M. Nieuwstadt and H. van Dop, Eds., Reidel, 37–68.
- Toba, Y., N. Iida, H. Kawamura, N. Ebuchi, and I. S. F. Jones, 1990: Wave dependence on sea-surface wind stress. *J. Phys. Oceanogr.*, **20**, 705–721.
- Wyngaard, J. C., 1973: On surface-layer turbulence. *Workshop on Micrometeorology*, D. A. Haugen, Ed., Amer. Meteor. Soc., 101–149.
- Yelland, M. J., and P. K. Taylor, 1996: Wind stress measurements from the open ocean. *J. Phys. Oceanogr.*, **26**, 541–558.